Protein Engineering, Design & Selection, 2015, vol. 28 no. 4, pp. 93–105
doi: 10.1093/protein/gzv005
Advance Access Publication Date: 25 February 2015
Original Article

OXFORD

Original Article

Receptor-targeted lentiviral vectors are exceptionally sensitive toward the biophysical properties of the displayed single-chain Fv

Thorsten Friedel[1], Lydia J. Hanisch[2], Anke Muth[1], Annemarie Honegger[3], Hinrich Abken[4,5], Andreas Plückthun[3], Christian J. Buchholz[1,*], and Irene C. Schneider[1]

[1]Section of Molecular Biotechnology and Gene Therapy, Paul-Ehrlich-Institut, Paul-Ehrlich-Str. 51-59, Langen 63225, Germany, [2]Roche Pharmaceutical Research and Early Development, Protein Engineering Group, Roche Innovation Center Zürich, Schlieren 8952, Switzerland, [3]Department of Biochemistry, University of Zürich, Zürich 8057, Switzerland, [4]Center for Molecular Medicine Cologne, University of Cologne, Cologne 50931, Germany, and [5]Department I of Internal Medicine, University Hospital Cologne, Cologne 50931, Germany

*To whom correspondence should be addressed. E-mail: christian.buchholz@pei.de
Edited by Steven Russell

Received 13 August 2014; Revised 4 December 2014; Accepted 27 January 2015

Abstract

An increasing number of applications require the expression of single-chain variable fragments (scFv) fusion proteins in mammalian cells at the cell surface membrane. Here we assessed the CD30-specific scFv HRS3, which is used in immunotherapy, for its ability to retarget lentiviral vectors (LVs) to CD30 and to mediate selective gene transfer into CD30-positive cells. Fused to the C-terminus of the type-II transmembrane protein hemagglutinin (H) of measles virus and expressed in LV packaging cells, gene transfer mediated by the released LV particles was inefficient. A series of point mutations in the scFv framework regions addressing its biophysical properties, which substantially improved production and increased the melting temperature without impairing its kinetic binding behavior to CD30, also improved the performance of LV particles. Gene transfer into CD30-positive cells increased ~100-fold due to improved transport of the H-scFv protein to the plasma membrane. Concomitantly, LV particle aggregation and syncytia formation in packaging cells were substantially reduced. The data suggest that syncytia formation can be triggered by trans-cellular dimerization of H-scFv proteins displayed on adjacent cells. Taken together, we show that the biophysical properties of the targeting ligand have a decisive role for the gene transfer efficiency of receptor-targeted LVs.

Key words: CD30, HRS3, lentiviral vector, particle aggregation, scFv interface

Introduction

Expression and stability of antibody single-chain variable fragments (scFv) in any system, prokaryotic and eukaryotic alike, faces the problem of aggregation competing with folding, and is thus strongly dependent on the primary sequence of the antibody (Wörn and Plückthun, 2001). While eukaryotic cells are in general more forgiving in the expression yields of aggregation-prone antibody fragments than bacteria (Schaefer and Plückthun, 2012), the stability against denaturation is a molecular property and thus independent of the producing host. A poor yield of *in vivo* folding (leading to aggregation and/or degradation in the producing cell) can lead to limited secreted production (Jäger *et al.*, 2013) or expression at the cell surface when fused to transmembrane proteins. The latter is relevant for cell surface display libraries (Doerner *et al.*, 2014), T cell receptors or chimeric antigen receptors (CARs)

retargeted to tumor antigens (Lipowska-Bhalla *et al.*, 2012; Rosenberg, 2012), and can be challenging for cell-type specific gene transfer with viral vectors. The solution must therefore lie in improving the properties of the antibody fragment by sequence engineering.

Viral vectors have become an important tool for the genetic modification of cells in basic research as well as molecular medicine. Lentiviral vectors (LVs) are unique in their ability to integrate the delivered gene permanently into the host cell's genome, thus producing a stable genetic modification not only in the initially transduced cell but also in any off-spring cells resulting from cell division or differentiation (Kaufmann *et al.*, 2013). Usually LVs are pseudotyped with glycoproteins mediating transduction of a broad spectrum of cells, such as the glycoprotein G of the vesicular stomatitis virus (VSV-G).

More and more applications, however, require selective transduction of a distinct cell-type present in a mixture of cells (*ex vivo* gene transfer) or in a particular organ (*in vivo* gene transfer). Examples include, but are not limited to, the delivery of small interfering RNA or transcription factors to modulate cell physiology, or suicide genes to eliminate unwanted cells. Two systems of such cell entry targeted LVs have been described, both relying on the destruction of the natural receptor usage and on displaying a targeting domain on the vector particle surface, i.e. a high-affinity ligand recognizing a cell surface marker that defines the cell population of choice (Buchholz *et al.*, 2009).

The system used here was initially established for oncolytic measles viruses (Nakamura *et al.*, 2005) and has then been extended to LVs (Anliker *et al.*, 2010). The scFv providing the receptor specificity is fused to the C-terminus of measles virus hemagglutinin (H protein), a type-II glycoprotein responsible for particle attachment to the cell entry receptor. H protein forms dimers that are composed of an N-terminal cytoplasmic tail, a large extracellular stem region and a two-blade propeller-shaped head (Colf *et al.*, 2007; Hashiguchi *et al.*, 2007). The exact position of the displayed scFv cannot be predicted, as structural information is not available for the ultimate C-terminal residues of H. Moreover, H protein bears point mutations to ablate its recognition sites for the natural measles virus receptors and is truncated in its cytoplasmic tail to allow LV particle incorporation. Cytoplasmic tail truncation is also necessary for the fusion protein F, which forms a complex with H and mediates fusion of the vector particle membrane with the host cell membrane upon receptor contact by H.

Specificity for the target cell surface receptor of choice is defined by the targeting domain fused to H which can be, besides an scFv, a designed ankyrin repeat protein (DARPin; Münch *et al.*, 2011), or a natural protein ligand (IL13; Ou *et al.*, 2012). This way, gene transfer mediated by such LVs has been restricted to a variety of cell types such as neurons, hematopoietic stem cells, tumor cells, subtypes of endothelial cells and lymphocytes, with very high selectivity (Funke *et al.*, 2009; Anliker *et al.*, 2010; Münch *et al.*, 2011; Zhou *et al.*, 2012; Abel *et al.*, 2013). The repertoire of cell types addressable by this approach appears to be limited by the availability of suitable targeting domains only. Among these, scFvs are preferred, since they are most easily available (can be cloned from hybridomas or phage display libraries), and in some cases special features of the parental antibody such as activation of cells upon antigen contact can be transferred to the vector particles (Zhou *et al.*, 2012; Kneissl *et al.*, 2013).

Antibody variable domains can be classified to particular subgroups according to their germline family, and these differ greatly in functional expression and stability (Ewert *et al.*, 2003b). The various complementarity determining regions (CDRs) further contribute to these properties—positively or negatively. Finally, affinity maturation during B cell development via somatic hypermutation will further change the sequence and thus the stability properties as well. Typically, mutations will be selected by the immune system for their contribution to increasing affinity (Klein *et al.*, 2013), yet mutations may also interfere with antibody stability and will be selected by the B cell as long as they are above a certain threshold. The effects on stability appear to be more pronounced in the scFv fragment than in the Fab fragment (or the full antibody) because the constant domains C_H1 and C_L have a stabilizing function to the linked variable regions and partially compensate for negative effects (Röthlisberger *et al.*, 2005). However, fusion proteins can only conveniently be made in the single-chain format.

Accordingly, yield, stability and resistance to aggregation of scFv cloned from antibodies can be improved by mutating back to the framework consensus (Forsberg *et al.*, 1997; Wörn and Plückthun, 2001; Chowdhury and Vasmatzis, 2003; Honegger, 2008). Additionally, there are distinct differences in the biophysical properties between the germline frameworks regarding thermodynamic stability of V_H and V_L chains individually and in various combinations (Ewert *et al.*, 2003b; Honegger *et al.*, 2009). Consequently, changes of some amino acids can be of benefit to frameworks with poor stability when adopted from frameworks with good biophysical properties (Ewert *et al.*, 2003a).

To be suitable as targeting domain on LVs, an scFv must fulfill many requirements such as the efficient transport to the cell surface and folding in the context of a type-II transmembrane fusion protein, high stability at 37°C, and high affinity for the targeted cell surface antigen. Therefore, the stability of an scFv used for receptor-targeted LVs should also greatly impact on the gene transfer activity of the vector. We tested this hypothesis by engineering a new receptor-targeted LV which delivers genes specifically into CD30-positive cells. The original CD30-specific scFv used was derived from the hybridoma line HRS3 (Hombach *et al.*, 1998), which had been employed as targeting domain of cytokines (Heuser *et al.*, 2004) and of a CAR for the therapy of Hodgkin's lymphoma (Hombach *et al.*, 1998; Heuser *et al.*, 2004). Here, we show that an optimized framework of the HRS3-scFv substantially enhances its cell surface transport, the yield of produced CD30-specific LVs and finally the efficiency in gene delivery into CD30-positive cells.

Material and methods

Plasmid construction

Starting from plasmid pHRS3-scFv (Hombach *et al.*, 1998), the coding sequence of the HRS3-scFv was cloned via SfiI/NotI restriction into plasmid backbone pCG-$H_{mut}\Delta18$ (Anliker *et al.*, 2010) providing the coding sequence for truncated and mutated measles virus H protein and for an additional $(G_4S)_3$ linker (L3) between H and the scFv resulting in plasmid pHL3-HRS3. HRS3 variants were obtained by mutation with the QuikChange® Multi Site Directed Mutagenesis Kit (Agilent Technologies). Primer details are available upon request. To introduce a His tag at the C-terminal end of H in scFv-free LVs, $pH_{WT}\Delta18$-His was cloned by replacing the PvuII-PstI fragment at the 3′-end of the H-coding region in $pH_{WT}\Delta18$-Fab7 (Anliker *et al.*, 2010) by a *de novo* synthesized DNA fragment (GeneArt, Invitrogen) containing the additional cloning sites SmaI, SfiI and NotI between H and the His tag coding sequence.

For plasmid pCR3.1-HRS3, the SfiI site in the backbone of pCR3.1-B1.8 (Sanz *et al.*, 2002) was destroyed via T4 polymerase fill-in. A PCR product obtained with primers ClaI-SfiI forward (5′-ATG GCA TCG ATG GCG GCC CAG CCG GCC ATG GCC CAG GTG CAA CTG CAG C-3′) and NotI reverse (5′-GGT GAT

GAG AAC CTC TTG CGG CCG C-3′) on the template pHL3-HRS3 was inserted via ClaI/NotI. All further scFv coding sequences were then exchanged via SfiI/NotI.

The coding sequence of the extracellular domain of CD30 was amplified by PCR with primers BssHII-CD30 forward (5′-CCT AGT GGC GCG CAC TCC ATG GCC TTC CCA CAG GAT CGA CCC-3′) and Not-CD30 reverse (5′-CAG ATA GCG GCC GCC TGG GTC CCC AGG GGT GG-3′) from plasmid pcDNA3.1-V5-His-Topo-CD30. The product was cut with BssHI and NotI and cloned into the mammalian expression plasmid pCMV-hIgGI-Fc-XP (kindly provided by Thomas Schirrmann, Braunschweig), providing a C-terminal human IgG-Fc tag, to obtain phuFc-CD30.

The coding sequence for the anti-His scFv 3D5 (Lindner *et al.*, 1997) was PCR amplified using the primers 3D5SfiI (5′-CCA GCA GGC CCA GCC GGC CGA CAT TTT GAT GAC CCA AAC-3′) and 3D5NotI (5′-CGG AGT CAG CGG CCG CCG CAG AGA CAG TGA CGG TAG-3′). The PCR product was inserted via SfiI/NotI into the plasmid pDisplay-$D^{9.29}$ (Rasbach *et al.*, 2013) to generate pDisplay-3D5.

Cell lines and cultivation

HEK293T, HT1080 and HT1080 derived cells were cultivated in Dulbecco's modified Eagle's medium (DMEM) supplemented with 10% fetal bovine serum (FBS) and 2 mM L-glutamine. Raji and HuT78 cells were grown in RPMI 1640 medium supplemented with 10% FBS and 2 mM L-glutamine.

HT1080-anti-His and HT1080-CD30 cells were established by stable transfection of HT1080 cells with polyethylenimine using pDisplay-3D5 and pcDNA3.1-V5-His-Topo-CD30, respectively, followed by G418 (Invitrogen, Karlsruhe, Germany) selection and single cell cloning for the HT1080-anti-His cells.

Vector particle production

Vector particles were generated as previously described (Rasbach *et al.*, 2013). In brief, HEK293T cells were transiently transfected using polyethylenimine (PEI). Twenty-four hours prior to transfection, 2×10^7 cells were seeded into a T175 flask. For standard production of HRS3opt1#5-LV and HRS3opt2#2-LV, 5.25 µg of the plasmid encoding $F_{WT}\Delta30$, 1.75 µg of the plasmid encoding an H variant, 14 µg of the packaging plasmid pCMVΔR8.9 (Zufferey *et al.*, 1997) and 14 µg of the transfer vector plasmid pSEW (Demaison *et al.*, 2002) encoding GFP were used. To obtain highest possible titers, the H to F plasmid ratio was adapted for each H-HRS3 variant: 6 µg H and 2 µg F for HRS3-LV, and 4 µg H and 4 µg F for HRS3opt1#3 and HRS3opt1#8-LV. MV-LV particles were produced by co-transfection of cells with 4 µg $pH_{WT}\Delta18$-His, 6.7 µg $pF_{WT}\Delta30$, 9 µg pCMVΔR8.9 and 9 µg pSEW. Vector particles pseudotyped with vesicular stomatitis virus G protein (VSVG) were produced by co-transfecting cells with 6.13 µg pMD2.G (kindly provided by Didier Trono, Lausanne, Switzerland), 11.38 µg pCMVΔR8.9 and 17.50 µg pSEW. Components were mixed together with 2.3 ml of DMEM without additives. The transfection reagent mix was prepared by mixing 140 µl of 18 mM PEI with 2.2 ml of DMEM without additives. This mixture was added quickly to the DNA mix, briefly vortexed, and incubated for 20 min at room temperature. The cell culture medium was replaced by 10 ml of DMEM with 15% FBS and 2 mM L-glutamine, and the transfection mix was added, resulting in 10% FBS total. After 24 h, the medium was exchanged to DMEM with 10% FBS and 2 mM L-glutamine. Two days after transfection, the cell supernatant containing the pseudotyped vectors was filtered (0.45 µm filter) and purified by ultracentrifugation at 100 000×*g* and 4°C over a 20% sucrose cushion for 3 h. The pellet was re-suspended in 100 µl phosphate-buffered saline (PBS).

The quantity of p24 gag in purified vector particle suspensions was determined using the RETROtek HIV p24 antigen enzyme-linked immunosorbent assay (ELISA) kit (ZeptoMetrix Corporation, Buffalo, NY) according to the manufacturer's instructions. LV-particle numbers were calculated from p24 amounts assuming an average of 2000 molecules p24 per lentiviral particle (Wilk *et al.*, 2001).

Production and purification of scFv and CD30-Fc

Proteins were expressed in HEK293T cells and purified from the cell culture medium. The day before transfection with PEI, 2×10^7 HEK293T cells were seeded in two 175 cm² flasks. Seventy micrograms of pCR3.1-HRS3 or phuFc-CD30 were incubated with PEI as described above and added to the cells. On the next day, medium was removed, cells were washed once, before serum-free PANSERIN 293A medium (Pan-Biotech) was added. Supernatants were harvested 48 and 72 h after transfection, cleared via filtration (0.45 µm) and stored at 4°C.

scFv was purified and concentrated by immobilized metal-ion affinity chromatography (IMAC) using HisTrap FF Crude columns (1 ml, GE Healthcare, Freiburg, Germany) in an HPLC system (Bioline, Knauer, Berlin, Germany), according to the manufacturer's instructions. CD30-Fc was purified via protein A affinity chromatography using a Sartobind® Protein A column (Sartorius, Göttingen, Germany) in an HPLC system according to the manufacturer's instructions. Protein concentration was calculated after measuring the absorption at 280 nm in a micro-volume photometer (A280 measurement, NanoDrop, Thermo Scientific).

SDS-PAGE, Coomassie staining and western blot

Western blot analysis of proteins and concentrated vector particles was performed as described previously (Münch *et al.*, 2011). In brief, samples were either heated in denaturing buffer containing 10% β-mercaptoethanol or loaded to the gel without heating in non-reducing Novex® Tris-Glycine SDS Sample Buffer (Invitrogen), separated by gel electrophoresis, and either directly stained with Coomassie Brilliant Blue or electrotransferred onto nitrocellulose membranes (Amersham Biosciences, Freiburg, Germany).

The membranes were incubated with rabbit anti-F serum (F 431, 1:2000), rabbit anti-H serum (H 606, 1:1000) or mouse anti-p24 monoclonal antibody (clone 38/8.7.47, 1:1000; Gentaur, Aachen, Germany) to detect F, H and p24 gag, respectively. scFv fragments were detected with a monoclonal anti-myc antibody (ab18185, Abcam, Cambridge, UK). Secondary antibodies conjugated with horseradish peroxidase (1:2000; DakoCytomation, Hamburg, Germany) were used. Signals were detected using the ECL plus western blotting detection system (GE Healthcare, Munich, Germany). Specific deglycosylation of N-glycans of purified scFv was performed using Protein Deglycosylation Mix (New England BioLabs) according to the manufacturer's protocol.

Surface plasmon resonance measurements

All experiments were performed at 25°C using PBST as running buffer (10 mM PBS, pH 7.4 and 0.005% (v/v) Tween 20). A ProteOn XPR36 biosensor equipped with GLC and GLM sensor chips and coupling reagents (10 mM sodium acetate, pH 4.5, sulfo-N-hydroxysuccinimide, 1-ethyl-3-(3-dimethylaminopropyl)-carbodiimide hydrochloride [EDC] and ethanolamine) was purchased from BioRad Inc. (Hercules, CA).

For surface plasmon resonance (SPR) measurements, purified HRS3 variants and CD30-Fc were dialyzed (MWCO 3000; Spektrum Labs) against PBS containing 0.001% Tween-20 at 4°C overnight.

Immobilizations were performed at 30 µl/min on a GLM chip. Monoclonal mouse anti-penta-His antibody (Qiagen) was coupled using a standard amine-coupling procedure: all six ligand channels were activated for 5 min with a mixture of EDC (200 mM) and sulfo-NHS (50 mM). Immediately after the surfaces were activated, monoclonal mouse anti-penta-His antibody (15 µg/ml, 10 mM sodium acetate, pH 4.5) was injected across all six channels for 4 min. Finally, channels were blocked with a 5 min injection of 1 M ethanolamine–HCl (pH 8.5). Final immobilization levels were ranging from 6000 to 6200 RU. The scFv variants were captured by simultaneous injection along five of the separate whole 'analyte' channels (15 µg/ml, 30 µl/min) for 3 min and resulted in similar levels, ranging from 580 to 600 RU; buffer was injected along the sixth channel to provide an 'in-line' blank for double referencing purposes.

One-shot kinetic measurements were performed by injection of a dilution series of CD30-Fc (0, 12.5, 25, 50, 100 and 200 nM, 50 µl/min) for 3 min along the ligand channels. Dissociation was monitored for 10 min. Kinetic data were analyzed in ProteOn Manager v. 2.1. Processing of the reaction spot data involved applying an interspot-reference and a double-reference step using an inline buffer blank (Myszka, 1999). The processed data from replicate one-shot injections were fit to a simple 1:1 Langmuir binding model without mass transport (O'Shannessy *et al.*, 1993).

Protein thermal shift assay

To determine the stability of the purified HRS3 variants, the Protein Thermal Shift™ Assay (Life Technologies™) was used according to the manufacturer's protocol in an ABI PRISM® 7900HT real-time PCR machine (Life Technologies™). Data were processed using Prism 5 software (GraphPad Software) and the protein melting temperatures were calculated as described previously (Niesen *et al.*, 2007).

Transduction of cells, FACS analysis and competition assay

To determine the titers of HRS3-LV and VSV-G-LV stocks, HT1080-CD30 cells were transduced by at least four serial dilutions of vector particles. GFP-positive cells were quantified after 2 days by flow cytometry. For this purpose, cells were washed twice using FACS wash buffer (containing PBS w/o Mg^{2+} and Ca^{2+}, 2% FBS and 0.5% NaN_3), fixed using FACS fix buffer (containing PBS w/o Mg^{2+} and Ca^{2+} with 1% formaldehyde) and stored at 4°C upon analysis. FACS analysis was performed using the LSRII flow cytometer (Becton Dickinson), and data were analyzed with FCS Express software (Denovo Software). For titer calculation, dilutions were selected that showed a linear correlation between dilution factor and number of GFP-positive cells. For detection of CD30 at the surface, washed cells were incubated with anti-CD30-PE antibody (Miltenyi Biotec, Bergisch Gladbach, Germany) or isotype control antibody at 4°C for 1 h, washed twice and fixed.

For the vector competition assay, different amounts of soluble CD30-Fc were incubated with the LV variants for 15 min at 37°C and then added to HT1080-CD30 cells. Two days after transduction, the percentage of GFP-positive cells was determined by flow cytometry and the transduction efficiency was normalized to that obtained without CD30-Fc treatment.

Immunofluorescence microscopy

For immunofluorescence of H protein variants, 4×10^4 HEK293T cells were seeded into one well of an 8-well chambered coverglass (LabTekII, Nunc, Wiesbaden, Germany). After 24 h, they were transfected with 0.25 µg of an H plasmid variant using FuGENE® HD Transfection Reagent (Promega) according to the manufacturer's instructions. On the next day, cells were washed with PBS once and fixed in PBS supplemented with 4% formaldehyde for 20 min at room temperature. Subsequently, cells were permeabilized with 0.5% Triton X-100 in PBS for 8 min at room temperature. After an additional washing step and blocking in 5% chicken serum in PBS for 45 min at room temperature, cells were incubated with anti-H (clone K83, 1:20; Liebert *et al.*, 1994) monoclonal antibody for 1 h at 37°C. Secondary antibody conjugated with Cy3 dye (anti-mouse IgG, 1:250; DAKO, Hamburg, Germany) was added and incubated for 1 h at 37°C. Then, cells were washed twice with PBS and analyzed using a laser scanning microscope (LSM510; Zeiss, Jena, Germany). Micrographs are shown as false-color images generated with LSM Image Browser (Zeiss, Jena, Germany).

Particle size measurement (nanoparticle tracking analysis)

Particle size measurement of LVs was performed using the NanoSight NS500 instrument (NANOSIGHT Ltd, Salisbury, UK). Vector stocks were adjusted to 10 pg p24/ml with degased PBS. Each sample was measured five times for 75 s at 24°C. NTA2.3 software (NANOSIGHT Ltd) was applied for particle identification and size analysis.

Sequence alignments and computational modeling

The sequence of HRS3-scFv was aligned to germline sequences with MS Excel with the macros and information provided at 'AAAAA, AHo's Amazing Atlas of Antibody Anatomy' at http://www.bioc.uzh.ch/antibody (Honegger and Plückthun, 2001b).

Computational modeling for HRS3opt2#2 was based on the scFvs PDB ID 2gki for V_H and V_L and PDB ID 1dl7 for the interface using the CPHmodels 3.2 Server which is online available at http://www.cbs.dtu.dk/services/CPHmodels/ (Nielsen *et al.*, 2010). The structural alignment, modifications to depict amino acids of HRS3 in the structure and visualization were performed with PyMOL (Schrödinger). The resulting structure was further modified by GlyProt available online at http://www.glycosciences.de/modeling/glyprot/ (Bohne-Lang and von der Lieth, 2005).

Statistical analysis

Results are expressed as mean ± SD. Data were considered statistically significant for $P < 0.05$. Differences were evaluated by Student's *t*-test. All statistical calculations were done using Prism 5 software (GraphPad Software).

Results

The HRS3-scFv was previously derived from the hybridoma line HRS3 (Hombach *et al.*, 1998) and has been used for anti-cancer therapeutic approaches (Heuser *et al.*, 2004; www.clinicaltrials.gov: NCT01192464 and NCT01316146). When applied as targeting domain on LVs as described for other scFvs (Anliker *et al.*, 2010), we detected selective gene transfer into a few CD30-positive cells by microscopy at very low frequencies, which were at least two orders of magnitude below that of other receptor-targeted LVs.

In order to improve the utility of the HRS3-scFv as targeting domain, we analyzed the sequence of the variable antibody regions and identified the heavy chain to belong to subgroup 1 (muV_{H1}) and the kappa light chain to subgroup 6 ($muV_{L\kappa6}$). When compared

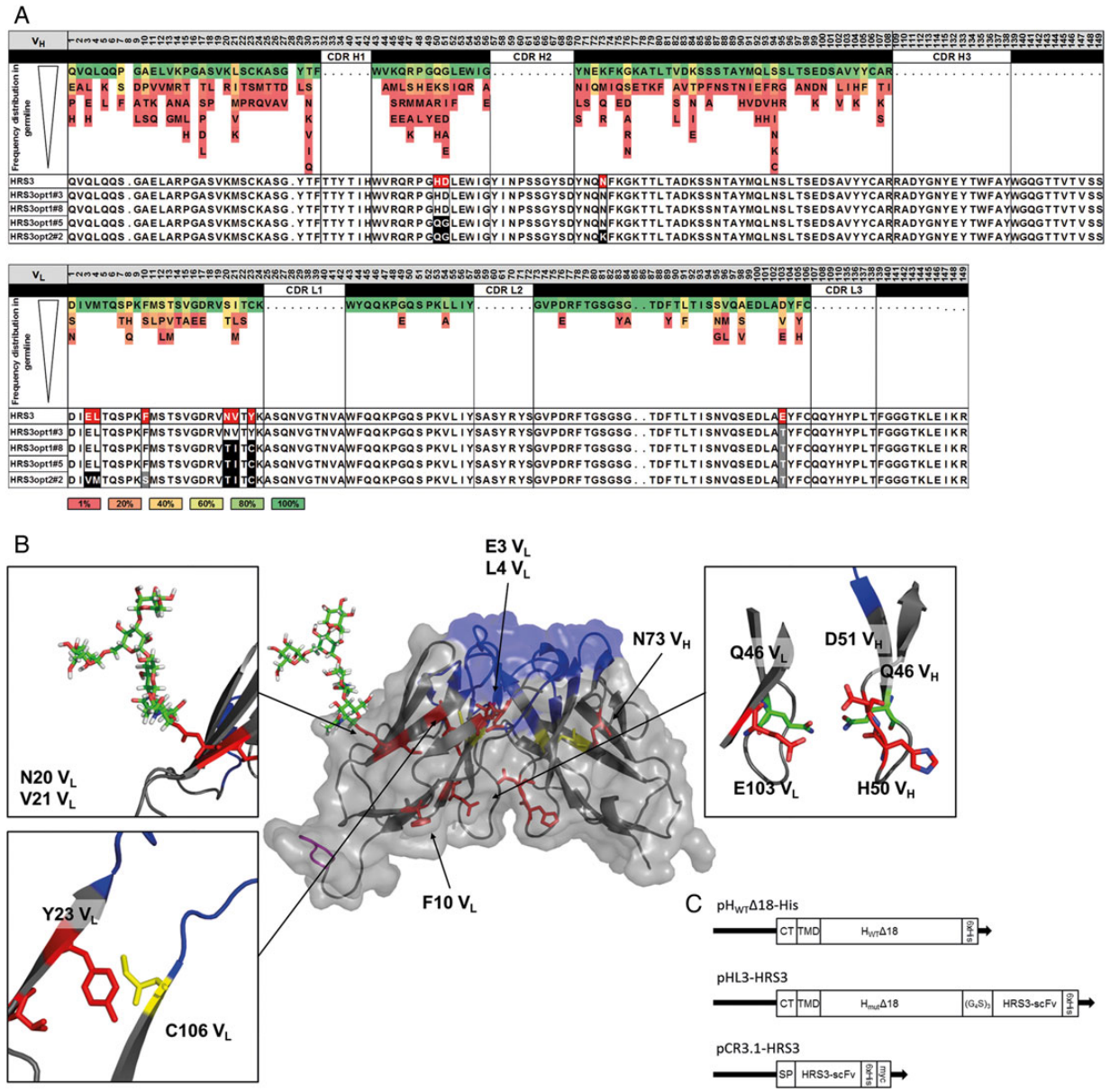

Fig. 1 Identification and repair of crucial residues in the framework regions of the CD30-specific scFv HRS3. (**A**) One hundred and twenty sequences of mV$_H$1 chains (upper panel) and 12 sequences of mV$_{L\kappa6}$ chains (lower panel) were aligned (uppermost sequence in each panel). Numbering of positions is according to Honegger and Plückthun (2001b). All residues of the framework regions occurring at least once at a particular position are listed with decreasing frequency from top to bottom with frequencies indicated by the color code. The sequences of the V$_H$ and V$_L$ chains of HRS3 and the HRS3 variants generated are depicted below. Amino acids in the HRS3 sequence differing from germline consensus are labeled in red. Residues in the HRS3 variants are highlighted in black when changed to consensus and in gray when changed to residues previously shown to enhance scFv stability. (**B**) Structure of HRS3 obtained by automated homology modeling. CDRs are labeled in blue, residues identified in (A) are labeled in red and cysteine residues in yellow. The positions of the His tag (purple) and the N-glycan (green) were estimated and modeled by PyMol. Enlargements depict in detail the missing cysteine bridge in V$_L$, position of the glycosylation and amino acids within the interface. (**C**) Schematic drawing of expression plasmids. Plasmid pHL3-HRS3 encodes the H-scFv fusion protein; pH$_{WT}$Δ18-His the H protein derived from a wild-type MV strain (Funke *et al.*, 2009) and pCR3.1-HRS3 were used for the expression of scFv in HEK293T cells as secreted protein. Immunological tags for detection (His and myc), the signal peptide (SP), the transmembrane domain (TMD) and cytoplasmic tail (CT) are indicated.

with the sequences of antibodies of matching murine germlines, as published by IMGT®, the international ImMunoGeneTics information system® (http://www.imgt.org) (Lefranc *et al.*, 1999), we identified several residues at highly conserved positions of the framework regions that differed from the germline consensus sequence (Fig. 1A and B). Additionally, both germlines carry residues which do not occur in well behaving antibodies. We thus focused here on mutating back germline liabilities in muV$_{H1}$ to versions found in well behaved subgroups and we mostly engineered the light chain back to its muV$_{L\kappa6}$ consensus.

Most of these non-germline residues may have been introduced by somatic hypermutation during B cell development. Additionally, especially at the beginning of the variable regions, changes are most likely introduced by mispairing of the primers used for PCR (E3/L4 V$_L$

instead of V3/M4 V_L), and further changes through PCR errors cannot be excluded.

The most dramatic alterations from the muV$_{L\kappa6}$ subgroup consensus in the light chain are a Cys → Tyr mutation at position 23, resulting in a disruption of the completely conserved disulfide bond (C23–C106 in V_L), as well as a mutation introducing a potential N-glycosylation site (N20, V21, T22 in V_L) in close vicinity of the disrupted disulfide bond. Furthermore, the muV$_{L\kappa6}$ subgroup germline is missing a common threonine (T103 V_L) present within the charge cluster of the well behaving subgroups (Ewert *et al.*, 2003a,b) (Fig. 1B).

Within the heavy chain, liabilities are present at the muV$_{H1}$ germline level: a histidine (H50 V_H) replaces a glutamine (Q50 V_H) and a charged aspartate (D51 V_H), the highly flexible non-polar glycine that is preferred for β-strand formation at this position (G51 V_H). Near the CDR2, a highly conserved lysine (K73 V_H) is substituted by asparagine (N73 V_H).

We hypothesized that these residues interfere with efficient folding, and thus with gene transfer by CD30-targeted LVs. Therefore, a series of HRS3-scFv variants was generated by reverting residues to germline consensus or to residues previously shown to enhance scFv production, stability and folding (Forsberg *et al.*, 1997; Honegger and Plückthun, 2001a; Ewert *et al.*, 2003a; Honegger, 2008) (Fig. 1A). HRS3opt1#3 only reintroduces the single residue T103 V_L, HRS3opt1#8 also reintroduces the disulfide and removes the glycosylation site, HRS3opt1#5, combines these and also adds two V_H mutations potentially affecting chain association, and finally HRS3opt2#2 adds additional mutations previously deduced. These variants were cloned into plasmid backbone pCR3.1 for secretion by transfected mammalian cells and into the pCG-H$_{mut}$Δ18-L3 plasmid backbone for expression as fusion protein with the H protein (Fig. 1C).

The secreted scFv variants were produced in the same cell system, i.e. HEK293T, as the targeted LVs. After transfection of the expression plasmids, the scFvs were harvested from the cell culture supernatant and purified by IMAC. Variant HRS3opt1#8, in which the disulfide bond has been restored and the putative glycosylation site had been mutated, was detected in cell lysate and cell culture supernatant by western blot analysis; however, it could not be purified by IMAC (data not shown), hinting at soluble aggregates. All other variants were readily expressed and purified with yields above that of HRS3-scFv. In fact, the yields increased with the number of 'corrected' residues from 79 µg for HRS3-scFv to 189 µg for HRS3opt2#2 per 175 cm² cell culture area (Table I). Gel electrophoretic analysis of the purified proteins revealed lower electrophoretic mobility for HRS3 and HRS3opt1#3 (Fig. 2A, lanes 1 and 2) when compared with HRS3opt1#5 and HRS3opt2#2 (Fig. 2A, lanes 3 and 4). This is in line with the presence of N-glycosylation in HRS3 and HRS3opt1#3 which was confirmed by enzymatic deglycosylation (Fig. 2B). Gel electrophoresis under non-reducing conditions revealed no insoluble aggregates and only small fractions of dimers for all variants (Fig. 2A, lanes 6–9).

To determine the thermal stability of the scFv variants, we used the fluorescence-based thermal shift assay in which the heat-induced unfolding process is monitored via a dye binding to hydrophobic residues that are inaccessible in the folded protein (Niesen *et al.*, 2007). The stability of the scFv variants increased up to 74°C for HRS3opt1#5 (Table I). For the wild-type HRS3-scFv, we did not detect any shift in fluorescence intensity over a temperature range from 25 to 95°C, indicating that this protein may be less stable already at room temperature.

While the introduced changes in the framework regions increased stability, they might also affect the binding affinity. Therefore, we assessed the CD30-binding properties of the scFv by SPR measurements. The extracellular domain of CD30 was expressed as a secreted variant in HEK293T cells, tagged with the dimerizing human Fc-domain (CD30-Fc) to facilitate purification and detection. The HRS3-scFv variants were captured by an immobilized anti-His antibody via their His tags with comparable efficiency (Supplementary Fig. S1A). The kinetic profile of the scFv/CD30 interaction was then determined by measuring the association and dissociation rates of the dimeric CD30-Fc. All scFv variants including the parental scFv showed similar binding behavior (Supplementary Fig. S1B) with apparent dissociation constants of 3.7–3.9 nM (Table II).

Having shown increased stability by the introduced mutations while keeping the binding behavior unchanged, we next analyzed the variants as fusion constructs with the measles virus H variant. To become incorporated into LV vector particles, it is crucial that the H-scFv proteins are efficiently expressed on the surface of the producer cells. We therefore determined the cell surface expression of the H-scFv proteins by flow cytometry and the subcellular localization by intracellular immunofluorescence after transfection into HEK293T cells. All variants were expressed at the cell surface without major differences as revealed by flow cytometry (data not shown), however differences were detectable at the intracellular level. While the unmodified HRS3-scFv and HRS3opt1#3 and HRS3opt1#8 mainly held back the H protein in intracellular vesicles and the endoplasmic reticulum (ER), H-HRS3opt1#5 and H-HRS3opt2#2 were predominantly located at the extracellular membrane (Fig. 3A), reflecting the best production and stability of these scFv when expressed as secreted

Table I. Main properties of the HRS3-scFv variants

	Yield (µg/175 cm²)	Melting temperature (°C)	Glycosylated	Particle number per ml[a]	Average particle size (nm)	Syncytia[b] formation	Functional titer[c] (t.u./ml)
HRS3	78.7	<25[d]	yes	7.6×10^{10}	133.3 ± 18.6	+++	3.1×10^{4}
HRS3opt1#3	126.1	66.4	yes	4.6×10^{11}	121.3 ± 6.6	++	6.9×10^{4}
HRS3opt1#8	n.d.[e]	n.d.	no	2.8×10^{11}	127.0 ± 7.4	+++	1.4×10^{4}
HRS3opt1#5	179.2	74.5	no	9.9×10^{11}	121.5 ± 5.9	+	1.5×10^{6}
HRS3opt2#2	188.8	71.9	no	1.0×10^{12}	123.78 ± 4.3	+	2.3×10^{6}

[a]Average values as determined by p24 ELISA, for standard deviations see Fig. 3.
[b]+++, strong syncytia formation; ++, moderate syncytia formation; +, residual/no syncytia formation as in MV-LV packaging cells.
[c]Average values as determined on HT1080-CD30 cells, for standard deviations see Fig. 4.
[d]Could not be determined by thermal shift assay.
[e]n.d., not determined.

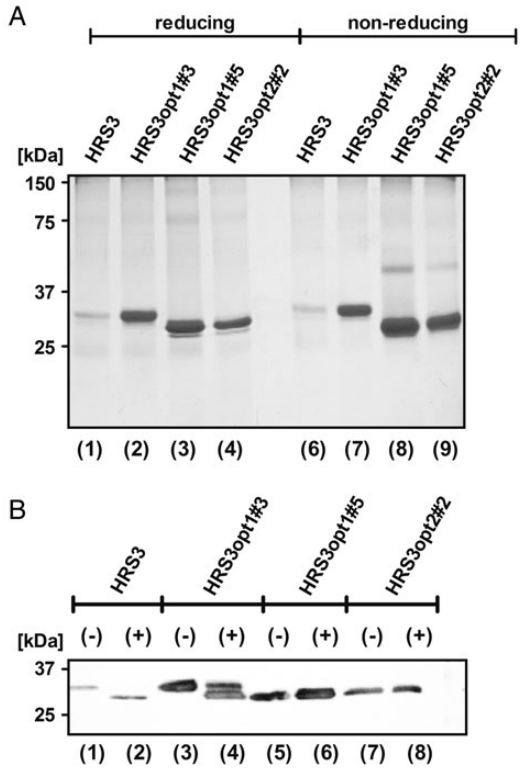

Fig. 2 Expression, purification and deglycosylation of HRS3-scFv variants. (**A**) The indicated scFv variants were expressed and secreted from HEK293T cells and purified from the cell culture supernatant by His tag affinity chromatography. For each variant, 20 µl from the main elution fraction was separated by SDS-polyacrylamide gel electrophoresis under reducing (lanes 1–4) and under non-reducing (lanes 6–9) conditions, respectively. Proteins were visualized by Coomassie Blue staining. (**B**) One microgram of purified scFv was incubated in presence (+) or absence (–) of Protein Deglycosylation Mix. Alterations in the molecular weight were analyzed by western blot analysis using an myc-tag specific antibody.

Table II. Binding of dimeric CD30-Fc to HRS3-scFv variants determined by SPR

	k_a [1/(M s)]	k_d (1/s)	K_D (M)	R_{max} (RU)	χ^2 (RU)
HRS3	1.16×10^5	4.30×10^{-4}	3.71×10^{-9}	128.26	20.18
HRS3opt1#3	1.22×10^5	4.52×10^{-4}	3.71×10^{-9}	171.88	20.76
HRS3opt1#5	9.75×10^4	3.81×10^{-4}	3.91×10^{-9}	198.11	34.56
HRS3opt2#2	1.08×10^5	4.06×10^{-4}	3.75×10^{-9}	197.34	23.72

proteins. This suggests that the eukaryotic secretory quality control (Benyair *et al.*, 2011) holds back variants HRS3-scFv and HRS3opt1#3 and HRS3opt1#8.

Upon transfection into packaging cells the variants H-HRS3 and H-HRS3opt1#8 reproducibly induced strong syncytia formation, and H-HRS3opt1#3 to a lesser extent (Fig. 3B). Cells expressing H-HRS3opt1#5 showed few and those expressing H-HRS3opt2#2 basically no syncytia. The viral vector particles were harvested from the supernatant of the producer cells and purified by sedimentation through a sucrose cushion. As a measure of viral vector particle content, the amount of the capsid protein p24 was determined. Highest p24 values and thus similar particle numbers as in LV stocks pseudotyped with untargeted measles virus glycoproteins (MV-LV) were present in stocks of HRS3opt1#5-LV and HRS3opt2#2-LV, intermediate levels in HRS3opt1#3-LV and HRS3opt1#8-LV, and low levels in HRS3-LV (Fig. 3C). Western blot analysis of the vector stocks confirmed that all vector types had incorporated the F and the H-scFv protein (Fig. 3D).

Next, we determined the particle number in viral vector stocks using the nanoparticle tracking analysis (NTA) technology (NanoSight NS500), which calculates the hydrodynamic size of single particles from their tracked diffusion velocity and therefore detects aggregated particles (Filipe *et al.*, 2010). We measured four independently produced vector stocks per variant. MV-LV particles included for comparison showed a Gaussian distribution with an average hydrodynamic diameter of 139.3 ± 7.6 nm, and most particles exhibited a diameter of 123.8 ± 4.3 nm (Fig. 3E and F). Importantly, the particle number for MV-LV stocks calculated via NTA did not differ from that determined by p24 ELISA (Fig. 3H), thus nicely confirming that we tracked p24-containing particles by NTA. This holds true also for the scFv-displaying viral vector particles with the exception of HRS3-LV and HRS3opt1#8-LV, for which we determined ~3- to 5-fold more particles by NTA than by p24 ELISA (Fig. 3H). The particle diameters differed significantly between the scFv-displaying vectors: whereas HRS3opt2#2-LV showed a homogeneous size distribution with an average value of 144.25 ± 6.5 nm resembling that of MV-LV particles, HRS3-LV showed an almost biphasic size distribution with an average diameter of 174.5 ± 21.6 nm (Fig. 3E and F). A particle diameter of 155 nm reflects the predicted size of two linked spherical particles, each with a diameter of 120 nm. Notably, in stocks of all variants the fraction of aggregated particles and their average diameter decreased with the number of altered residues (Fig. 3F and G).

The *gfp* gene transferred by the vectors allowed the calculation of the titer of each stock as transducing units per ml (t.u./ml) by determining the amount of GFP-positive cells 48 h after transduction. As target cells we used HT1080 cells engineered to express human CD30 (HT1080-CD30) or a membrane-bound scFv recognizing the His tag (HT1080-anti-His) at the C-terminus of the HRS3-scFv (Fig. 4A). All LVs carrying an engineered scFv showed substantially enhanced titers on both cell lines when compared with HRS3-LV. The gene transfer efficiency mediated by the best variant, HRS3opt2#2-LV, was ~100-fold enhanced over HRS3 on HT1080-CD30 (Fig. 4B) and ~25-fold enhanced on HT1080-anti-His cells (Fig. 4C).

Interestingly, with the exception of MV-LV, all vectors transduced HT1080-anti-His cells considerably more efficiently than HT1080-CD30 cells. The difference was especially pronounced for HRS3-LV, HRS3opt1#3-LV and HRS3opt1#8-LV. Normalizing the transduction rates to p24 amounts (rel. transduction) revealed that on HT1080-anti-His cells the differences in transduction rates were mainly reflected by the particle numbers present in the viral vector stocks. On HT1080-CD30 cells, in contrast, the relative transduction mediated by HRS3opt1#5-LV and HRS3opt2#2-LV was ~10-fold more efficient than that of HRS3-LV (Fig. 4D and E). Thus, the modifications introduced into the scFv framework regions did not only enhance particle release from packaging cells but also cell entry of vector particles via CD30.

To prove cell-type specificity of the viral vector with the highest titer (HRS3opt2#2-LV), cells with different levels of CD30 expression were identified (Fig. 5A). HuT78 cells, naturally expressing CD30, were used as target cells besides HT1080-CD30 for gene delivery. As non-target cells, CD30-negative HT1080 and Raji cells were incubated with HRS3opt2#2-LV. For comparison, vector particles pseudotyped with the non-selective envelope glycoprotein VSV-G were used. While VSVG-LV transduced both CD30-positive and

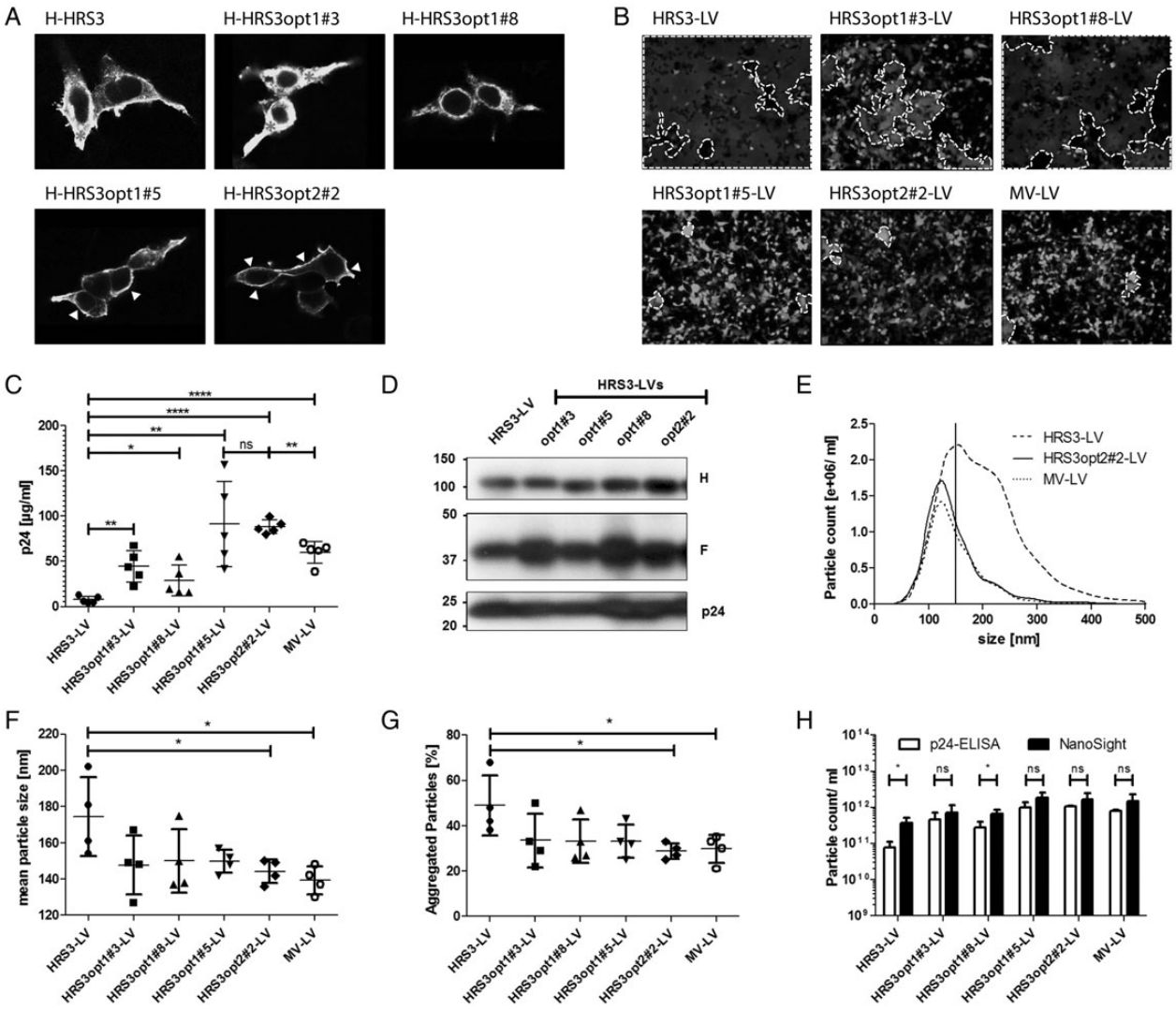

Fig. 3 Characterization of vector packaging cells and LV particles. (**A**) Immunofluorescence staining of the indicated H-HRS3 variants expressed in HEK293T cells using an H-protein specific antibody. Samples were analyzed 1 day after transfection. Asterisks indicate the presence of H-HRS3 proteins in intracellular compartments; arrowheads show localization at the plasma membrane (100-fold magnification). (**B**) Representative GFP fluorescence microscopic pictures of packaging cells producing the indicated LV types. Pictures were taken 48 h after transfection. Syncytia are labeled by dashed lines. (**C**) The amounts of p24 capsid protein in the indicated LV stocks as determined by quantitative ELISA. $n = 5$; mean values ± SD are shown; $^{*}P < 0.05$; $^{**}P < 0.01$; $^{***}P < 0.001$; n.s., not significant by unpaired *t*-test. (**D**) Incorporation of H-scFv and F proteins in the indicated LV stocks as determined by western blot using the H-specific antibody H606 (top panel), the F-specific antibody F431 (center panel) and a p24-specific antibody (bottom panel). (**E–G**) NTA analysis of particle size. (E) Size distribution (diameter) of representative stocks of HRS3-LV, HRS3opt2#2-LV and MV-LV. The vertical line indicates the threshold for aggregated particles, assuming that aggregation results in a diameter increase of at least 25% when two spherical particles each of a diameter of 120 nm aggregate. (F) Mean particle diameter of four independent stocks per variant and (G) percentage of aggregated particles. (**H**) Comparison of particle quantification via p24-ELISA (white bars) and NTA (black bars). The amounts of p24 were converted to particle numbers assuming 2000 p24 molecules per particle (Wilk *et al.*, 2001). Statistics for (E–H): $n = 4$; mean ± SD is shown; $^{*}P < 0.05$; $^{**}P < 0.01$; $^{***}P < 0.001$; n.s., not significant by unpaired *t*-test.

CD30-negative cells, only CD30-positive cells showed expression of GFP after incubation with HRS3opt2#2-LV (Fig. 5B). Flow cytometry data on GFP expression levels on all vector variants confirm the substantial increase in vector transduction achieved by engineering of HRS3 while retaining target receptor selectivity (Supplementary Fig. S2). Overall, GFP expression levels in transduced HuT78 cells were substantially lower than in HT1080-CD30 cells, which nicely correlate with the CD30 expression levels in these cells (compare Fig. 5A and B). Moreover, gene transfer into HT1080-CD30 cells by HRS3opt2#2-LV was efficiently blocked with increasing amounts of soluble CD30-Fc protein while VSVG-LV mediated transduction remained unaffected (Fig. 5C). These data demonstrate that cell entry of HRS3opt2#2-LV relies on the binding of vector particles to CD30.

Discussion

Here we investigated whether a CD30-specific scFv, which has shown unsatisfactory performance in the retargeting of LVs, can be rescued by introducing suitable framework mutations. Remarkably, the introduced mutations converted the basically inactive parental HRS3-scFv into an scFv that mediated efficient and specific gene delivery into CD30-positive cells, thus demonstrating that framework

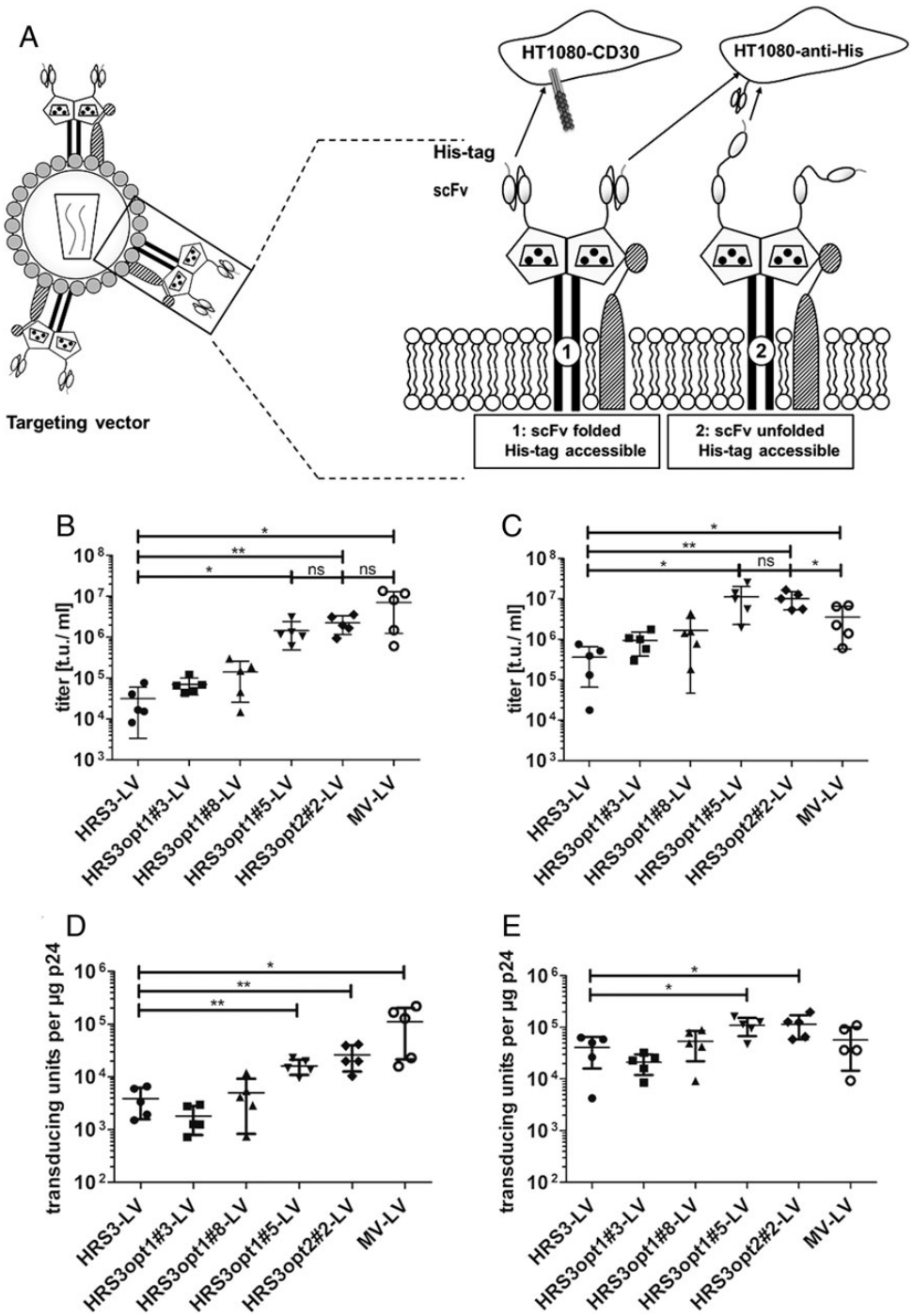

Fig. 4 Gene transfer titers of vector stocks. (**A**) Schematic drawing of scFv-displaying LV, the H-scFv/F glycoprotein complex and target cells. The H-scFv protein is depicted as dimer with a stalk domain inserted in the plasma membrane and globular heads displaying the scFv and carrying point mutations that inactivate natural receptor binding ('blinding' symbolized by dotted trapezium). The trimeric F protein is shown as monomer in complex with H-scFv. Vector particles enter HT1080-CD30 cells via CD30, HT1080-anti-His via the cell-surface-displayed His-tag-specific scFv 3D5. While stable scFv mediate LV entry into both cell types, LVs displaying unfolded scFv only enter HT1080-anti-His cells. (**B–E**) Titers of scFv displaying LVs were determined on HT1080-CD30 (B and D) or HT1080-anti-His (C and E) cells by quantifying GFP gene transfer in a dilution series of vector stocks. Titers of MV-LV stocks were determined on Raji cells (B and D) besides HT1080-anti-His cells. Relative titers (D and E) were determined by normalizing the amounts of transducing units (t.u./ml) to the p24 amounts. $n = 5$; mean ± SD is shown; $^{*}P < 0.05$; $^{**}P < 0.01$; n.s., not significant by unpaired *t*-test.

modifications can improve scFvs applied for receptor-targeted LVs. To get a comprehensive picture about the impact of the introduced mutations on the molecular level, we characterized both the LV particles displaying the scFv variants and the scFvs themselves as secreted proteins released from transfected HEK293T cells. The introduced changes, designed to improve the biophysical properties of the scFv not only increased thermostability and expression of the scFv in HEK293T cells but also reduced aggregation of vector particles and

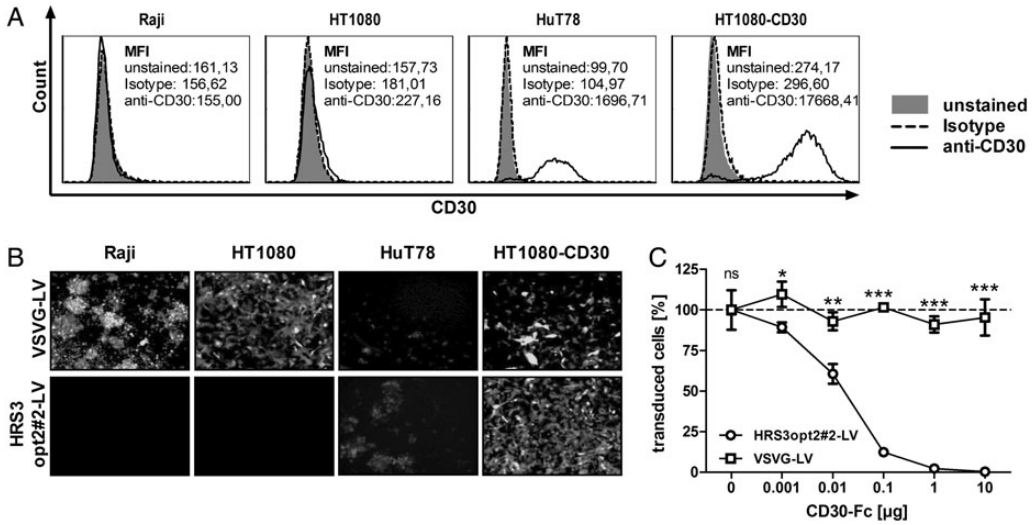

Fig. 5 Specificity of the CD30-targeted LV. (**A**) CD30 surface expression levels in Raji, HT1080, HuT78 and HT1080-CD30 cells were determined by flow cytometry using the CD30-specific antibody anti-CD30-PE (Miltenyi Biotec, black lines). As controls, cells were analyzed unstained (filled gray areas) or incubated with an isotype control antibody (dashed lines). The mean fluorescence intensities (MFIs) are provided for each cell type and histogram. (**B**) CD30-positive (HT1080-CD30, HuT78) and CD30-negative (HT1080, Raji) cells were incubated with VSVG-LV or HRS3opt2#2-LV each applied at a dose of 1 t.u. per cell (MOI 1). Transduced cells were analyzed by fluorescence microscopy for GFP expression 48 h later. (**C**) Increasing amounts of soluble CD30-Fc protein were used to compete with transduction mediated by HRS3opt2#2 and VSVG-LV on HT1080-CD30 cells (MOI 1). The percentage of transduced cells is shown relative to that observed without CD30-Fc. $n = 3$; mean ± SD is shown; $^{*}P < 0.05$; $^{**}P < 0.01$; $^{***}P < 0.001$; $^{****}P < 0.0001$; n.s., not significant by unpaired *t*-test.

syncytia formation in the packaging cells. Our work therefore directly shows that the biophysical properties of the targeting molecule have implications for the generation of targeted LVs.

We investigated a series of HRS3-scFv variants containing an increasing number of modified residues in the framework regions of the V_L and V_H chains. The reasons for this strategy are 2-fold: First, the CDRs which determine binding affinity and specificity remain untouched. Secondly, these strategies are generic and not limited to a given antibody.

Thermostability of the soluble scFv benefitted most from the introduced mutation E103T V_L. There is a strong preference for amino acids with β-branched side chains (Thr, Val, Ile) at this position favoring β-strand conformation (Zhu and Blundell, 1996) while the glutamate side chain likely extends to the interface of V_H/V_L in close proximity to Q46 V_L-Q46 V_H which are stabilizing the interface (Fig. 1B). Improvements on the vector particle level, in contrast, became most obvious when residues HD50/51QG in V_H were repaired (Table I). Interestingly, D51 is localized in the periphery to the V_H/V_L interface close to Q46 V_L-Q46 V_H as well, but in contrast to E103, it belongs to the V_H chain (Fig. 1B), suggesting that this exchange further improved the inter-domain stability.

The two most prominent deviations from consensus in HRS3 are located in the V_L chain: the (unintended) glycosylation at residue N20, which is present as demonstrated by our data, and the Tyr substitution of C23 that forms a disulfide bridge with C106, which is totally conserved across all antibodies and is a major determinant of stability. For the corresponding disulfide bridge in V_H, it was previously demonstrated that the presence of a tyrosine instead of cysteine at position 106 results in overpacking of the core and thus strong destabilization of the scFv (Proba *et al.*, 1997). Most likely, Y23 twists outward to relieve overpacking and the glycosylation of N20 in V_L helps to limit the perturbation of the β strand to the C-terminal end of the strand. Yet, HRS3-opt1#8 in which we reconstituted the cysteine bridge (Y23C) and removed the glycosylation site in V_L (N20V/T21I) showed, if at all, only minor improvements compared with HRS3, despite the E103T mutation that benefitted HRS3-opt1#3. The absence of the glycosylation site was, however, tolerated once the V_H/V_L interface was further stabilized in HRS3opt1#5, which is consistent with previously published findings that the domains can stabilize each other (Wörn and Plückthun, 1998; Jäger and Plückthun, 1999a). Thus, V_L appears to have been the limiting factor for the stability of the whole scFv. It is therefore likely, that the accidental presence of an N-glycosylation could overcome the other defects of the overall unstable V_L, thus enabling the successful use of HRS3 as targeting domain in CARs (Hombach *et al.*, 1998). Glycosylation introduces a protein to the ER quality control (Benyair *et al.*, 2011), which is normally secured by the presence of N-glycosylation in the C_H2 domain of IgG. Since this antibody was cloned from a hybridoma, the original IgG must have had both deviations, and thus the B cell probably already selected N-glycosylation as a compensation for the other framework defects. That glycosylation can facilitate folding and increase solubility is well documented for other proteins and also scFvs (Lizak *et al.*, 2011).

A remarkable result of this work is the strongly reduced or even lost formation of syncytia in the vector packaging cells with variants HRS3opt1#5 and HRS3opt2#2. The reduction of syncytia formation correlated with strongly increased viral vector particle release and improved gene transfer rates. How can a few changes in the framework regions of an scFv make such a difference for syncytia formation? In principle, syncytia form, once the F protein has been activated by the H protein after receptor contact, irrespectively if H protein itself or the targeting domain (here the scFv) have attached to the target cell by binding the targeted cell surface receptor (Nakamura *et al.*, 2005). Interestingly, membrane fusion can also be activated if the targeting domain is not directly linked to H protein but presented as a separate third component within the vector envelope (Rasbach *et al.*, 2013). HEK293T packaging cells, however, are CD30 negative. The syncytia formed by packaging cells producing, e.g. HRS3-LV or HRS3opt1#8-LV,

therefore, cannot be due to CD30 binding. Thus, another trigger has to be considered. It is well established that reduced interface stability between V_H and V_L leads to the dimerization of scFv, especially, if their local concentration is high (Wörn and Plückthun, 2001). Each viral vector-producing cell expresses a high density of H-scFv proteins at its surface and is in tight contact with neighboring cells. Therefore, the scFv displayed on H may form a dimer with an scFv from a neighboring cell, thus providing the required receptor contact for H protein to activate F and trigger cell-to-cell fusion (Fig. 6). Alternatively, neighboring cells may have been connected to each other via hydrophobic residues exposed after unfolding of one domain, which is especially likely after opening of the interface. Previous studies demonstrated that for cell-to-cell fusion to proceed, a density of 10^4 receptor molecules per cell can be sufficient (Hasegawa *et al.*, 2007; Münch *et al.*, 2011). Moreover, the affinity of H protein for the MV receptor CD46 is rather low with 1×10^{-7} M when compared with that of other viruses such as HIV (10^{-8} M for CD4) (Santiago *et al.*, 2002; Wang, 2002) and lies within the range of the association constants between the V_L and V_H chains (Horne *et al.*, 1982; Jäger and Plückthun, 1999b). It is thus conceivable that trans-dimerization of scFvs displayed on adjacent cell membranes can indeed trigger cell-to-cell fusion and may therefore be preferred over cis-dimerization between scFv present on the same cell.

This hypothesis also explains the reduced syncytia formation observed for variants HRS3opt1#5 and HRS3opt2#2. These scFvs gave higher yields in mammalian cells, had a substantially increased thermal stability, and when displayed on vector particles, mediated gene transfer via the targeted receptor CD30 as efficiently as via a membrane-bound His-tag-specific scFv. It is reasonable that the His tag fused to the scFv C-terminus can attach LV particles to cells displaying a His-tag-specific scFv even if the scFv displayed on H is misfolded or unstable. Interestingly, the enhanced V_H/V_L interface stability seems to have influenced the cellular localization of the H-scFv protein as well: H-HRS3opt1#5 and H-HRS3opt2#2 showed a dramatic change in cellular localization toward the cell membrane while the strong intracellular staining observed for H-HRS3 indicates that this protein accumulated in the Golgi, ER or aggresomes (Kopito and Sitia, 2000), fully consistent with the action of the secretory quality control of eukaryotic cells (Benyair *et al.*, 2011).

Another line of evidence for the formation of scFv dimers across cells, i.e. between H-HRS3 proteins present on opposing membranes, was revealed by laser-based NTA based on Brownian motion. Only very few reports used this approach before for the quantification of lentiviral particles (Gutiérrez-Granados *et al.*, 2013; Papanikolaou *et al.*, 2013). Our data are well in line with the study by Gutiérrez-Granados *et al.* (2013) with respect to particle size and the compliance of particle numbers determined by NTA and p24-specific ELISA. NTA can thus be considered as additional or alternative method for the quality control of LV stocks. Interestingly, the diameter and the p24 content-normalized number of particles were significantly increased in batches of HRS3- and HRS-3opt1#8-LV, both vector particles displaying rather instable scFv. Possible explanations include, but are not limited to, enforced aggregation of particles due to scFv instability and release of apoptotic vesicles (Théry *et al.*, 2009), especially from syncytia. Notably, aggregation was greatly reduced already by the single framework mutation in HRS3opt1#3 as for all other HRS3 variants. Thus, particle aggregation seems to be less sensitive toward scFv instability than cell-to-cell fusion.

Taken together, our data support the importance of the biophysical properties of the protein exposed on the surface of LVs, in this case, the thermal and interface stability of scFv used for the retargeting. Low vector titers and strong syncytia formation in packaging cells can be overcome by stability engineering of the antibody framework regions. Sequence alignments of the V_L and V_H chains to germline consensus can be a straightforward approach to identify and repair destabilizing residues (Wörn and Plückthun, 2001; Ewert *et al.*, 2003a). Likewise, this approach can improve the yield of scFv upon expression in all cells, including mammalian cells. Besides, it will be informative to assess if the scFv identified here as optimal for the display on LVs will also be beneficial as targeting domains for CARs, for which an influence of the displayed scFv on their surface expression has

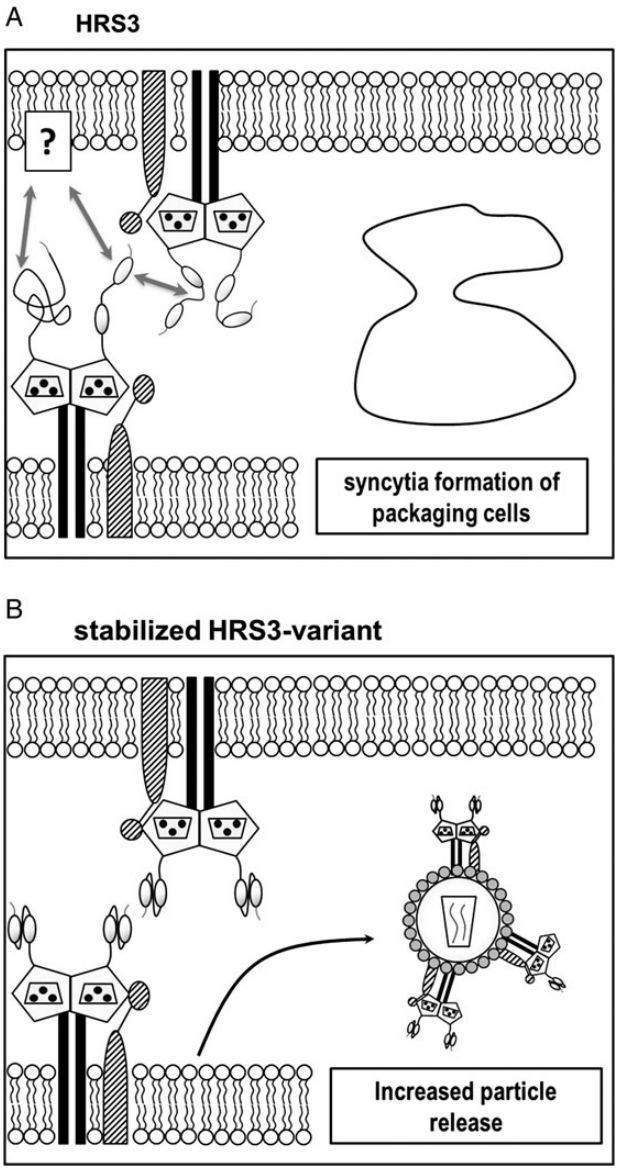

Fig. 6 Working model to explain syncytia induction in packaging cells expressing instable scFv. The H-HRS3 protein is depicted as dimer with a stalk domain inserted in the plasma membranes of neighboring cells and with globular heads displaying the scFv and carrying point mutations that inactivate natural receptor binding ('blinding' symbolized by dotted trapezium). The trimeric F protein is shown as monomer in complex with H-HRS3. (**A**) Membrane fusion and thus syncytia formation is triggered by dimerization of instable scFv displayed on neighboring packaging cells or by exposed hydrophobic residues (indicated by coiled lines) contacting unidentified parts of the neighboring cell. (**B**) When a stabilized HRS3 variant is displayed, syncytia formation is abolished and vector particle release enhanced.

previously also been demonstrated (Alonso-Camino *et al.*, 2013; Lipowska-Bhalla *et al.*, 2013). Independently from this, the scFv HRS3opt2#2 described here may serve as targeting domain not only for LVs but also for oncolytic measles viruses and possibly be applied for novel therapeutic strategies to target CD30-positive tumors such as Hodgkin lymphoma.

In more general terms, the LVs are surprisingly sensitive against the aggregation tendency of the displayed targeting protein. Therefore, the use of stability-engineered antibody fragments or the use of scaffold proteins, where the whole library has been engineered for good biophysical properties, such as DARPins (Boersma and Plückthun, 2011; Münch *et al.*, 2011), may be an important component in the further development of viral receptor targeting.

Supplementary data

Supplementary data are available at *PEDS* online.

Acknowledgement

We thank Gundula Braun and Ruth Freiling for excellent technical assistance.

Funding

This work was supported by the LOEWE Center for Cell and Gene Therapy Frankfurt funded by Hessisches Ministerium für Wissenschaft und Kunst (III L 4-518/17.004 (2010)) to C.J.B. and I.C.S.

References

Abel,T., El Filali,E.,, Waern,J., *et al.* (2013) *Blood*, **122**, 2030–2038.

Alonso-Camino,V., Sánchez-Martín,D., Compte,M., Nuñez-Prado,N., Diaz, R.M., Vile,R. and Alvarez-Vallina,L. (2013) *Mol. Ther. Nucleic Acids*, **2**, e93.

Anliker,B., Abel,T.,, Kneissl,S., *et al.* (2010) *Nat. Methods*, **7**, 929–935.

Benyair,R., Ron,E. and Lederkremer,G.Z. (2011) *Int. Rev. Cell Mol. Biol.*, **292**, 197–280.

Boersma,Y.L. and Plückthun,A. (2011) *Curr. Opin. Biotechnol.*, **22**, 849–857.

Bohne-Lang,A. and von der Lieth,C.-W. (2005) *Nucleic Acids Res.*, **33**, W214–W219.

Buchholz,C.J., Mühlebach,M.D. and Cichutek,K. (2009) *Trends Biotechnol*, **27**, 259–265.

Chowdhury,P.S. and Vasmatzis,G. (2003) *Methods Mol. Biol.*, **207**, 237–254.

Colf,L.A., Juo,Z.S. and Garcia,K.C. (2007) *Nat. Struct. Mol. Biol.*, **14**, 1227–1228.

Demaison,C., Parsley,K., Brouns,G., Scherr,M., Battmer,K., Kinnon,C., Grez, M. and Thrasher,A.J. (2002) *Hum. Gene Ther.*, **13**, 803–813.

Doerner,A., Rhiel,L., Zielonka,S. and Kolmar,H. (2014) *FEBS Lett.*, **588**, 278–287.

Ewert,S., Honegger,A. and Plückthun,A. (2003a) *Biochemistry*, **42**, 1517–1528.

Ewert,S., Huber,T., Honegger,A. and Plückthun,A. (2003b) *J. Mol. Biol.*, **325**, 531–553.

Filipe,V., Hawe,A. and Jiskoot,W. (2010) *Pharm. Res.*, **27**, 796–810.

Forsberg,G., Forsgren,M., Jaki,M., Norin,M., Sterky,C., Enhörning,A., Larsson,K., Ericsson,M. and Björk,P. (1997) *J. Biol. Chem.*, **272**, 12430–12436.

Funke,S., Schneider,I.C., Glaser,S., Mühlebach,M.D., Moritz,T., Cattaneo,R., Cichutek,K. and Buchholz,C.J. (2009) *Gene Ther.*, **16**, 700–705.

Gutiérrez-Granados,S., Cervera,L., Gòdia,F., Carrillo,J. and Segura,M.M. (2013) *J. Virol. Methods*, **193**, 85–95.

Hasegawa,K., Hu,C., Nakamura,T., Marks,J.D., Russell,S.J. and Peng,K.-W. (2007) *J. Virol.*, **81**, 13149–13157.

Hashiguchi,T., Kajikawa,M., Maita,N., Takeda,M., Kuroki,K., Sasaki,K., Kohda,D., Yanagi,Y. and Maenaka,K. (2007) *Proc. Natl Acad. Sci. U.S. A.*, **104**, 19535–19540.

Heuser,C., Guhlke,S., Matthies,A., Bender,H., Barth,S., Diehl,V., Abken,H. and Hombach,A. (2004) *Int. J. Cancer*, **110**, 386–394.

Hombach,A., Heuser,C., Sircar,R., Tillmann,T., Diehl,V., Pohl,C. and Abken, H. (1998) *Cancer Res.*, **58**, 1116–1119.

Honegger,A. (2008) *Handb. Exp. Pharmacol.*, **181**, 47–68.

Honegger,A. and Plückthun,A. (2001a) *J. Mol. Biol.*, **309**, 687–699.

Honegger,A. and Plückthun,A. (2001b) *J. Mol. Biol.*, **309**, 657–670.

Honegger,A., Malebranche,A.D., Röthlisberger,D. and Plückthun,A. (2009) *Protein Eng. Des. Sel.*, **22**, 121–134.

Horne,C., Klein,M., Polidoulis,I. and Dorrington,K.J. (1982) *J. Immunol.*, **129**, 660–664.

Jäger,M. and Plückthun,A. (1999a) *FEBS Lett.*, **462**, 307–312.

Jäger,M. and Plückthun,A. (1999b) *J. Mol. Biol.*, **285**, 2005–2019.

Jäger,V., Büssow,K., Wagner,A., Weber,S., Hust,M., Frenzel,A. and Schirrmann,T. (2013) *BMC Biotechnol.*, **13**, 52.

Kaufmann,K.B., Büning,H., Galy,A., Schambach,A. and Grez,M. (2013) *EMBO Mol. Med.*, **5**, 1642–1661.

Klein,F., Diskin,R.,, Scheid,J.F., *et al.* (2013) *Cell*, **153**, 126–138.

Kneissl,S., Zhou,Q., Schwenkert,M., Cosset,F.-L., Verhoeyen,E. and Buchholz, C.J. (2013) *PLoS ONE*, **8**, e79047.

Kopito,R.R. and Sitia,R. (2000) *EMBO Rep.*, **1**, 225–231.

Lefranc,M.-P., Giudicelli,V., Ginestoux,C., Bodmer,J., Muller,W., Bontrop,R., Lemaitre,M., Malik,A., Barbie,V. and Chaume,D. (1999) *Nucleic Acids Res.*, **27**, 209–212.

Liebert,U.G., Flanagan,S.G., Löffler,S., Baczko,K., ter Meulen,V. and Rima,B. K. (1994) *J. Virol.*, **68**, 1486–1493.

Lindner,P., Bauer,K., Krebber,A., Nieba,L., Kremmer,E., Krebber,C., Honegger, A., Klinger,B., Mocikat,R. and Plückthun,A. (1997) *BioTechniques*, **22**, 140–149.

Lipowska-Bhalla,G., Gilham,D.E., Hawkins,R.E. and Rothwell,D.G. (2012) *Cancer Immunol. Immunother.*, **61**, 953–962.

Lipowska-Bhalla,G., Gilham,D.E., Hawkins,R.E. and Rothwell,D.G. (2013) *Hum. Gene Ther. Methods*, **24**, 381–391.

Lizak,C., Fan,Y.-Y., Weber,T.C. and Aebi,M. (2011) *Bioconjug. Chem.*, **22**, 488–496.

Münch,R.C., Mühlebach,M.D., Schaser,T., Kneissl,S., Jost,C., Plückthun,A., Cichutek,K. and Buchholz,C.J. (2011) *Mol. Ther*, **19**, 686–693.

Myszka,D.G. (1999) *J. Mol. Recognit.*, **12**, 279–284.

Nakamura,T., Peng,K.-W., Harvey,M., Greiner,S., Lorimer,I.A.J., James,C.D. and Russell,S.J. (2005) *Nat. Biotechnol.*, **23**, 209–214.

Niesen,F.H., Berglund,H. and Vedadi,M. (2007) *Nat. Protoc.*, **2**, 2212–2221.

Nielsen,M., Lundegaard,C., Lund,O. and Petersen,T.N. (2010) *Nucleic Acids Res.*, **38**, W576–W581.

O'Shannessy,D.J., Brigham-Burke,M., Soneson,K.K., Hensley,P. and Brooks,I. (1993) *Anal. Biochem.*, **212**, 457–468.

Ou,W., Marino,M.P., Suzuki,A., Joshi,B., Husain,S.R., Maisner,A., Galanis,E., Puri,R.K. and Reiser,J. (2012) *Hum. Gene Ther. Methods*, **23**, 137–147.

Papanikolaou,E., Kontostathi,G., Drakopoulou,E., Georgomanoli,M., Stamateris,E., Vougas,K., Vlahou,A., Maloy,A., Ware,M. and Anagnou,N.P. (2013) *Virus Res.*, **175**, 1–11.

Proba,K., Honegger,A. and Plückthun,A. (1997) *J. Mol. Biol.*, **265**, 161–172.

Rasbach,A., Abel,T., Munch,R.C., Boller,K., Schneider-Schaulies,J. and Buchholz,C.J. (2013) *J. Virol.*, **87**, 6246–6256.

Rosenberg,S.A. (2012) *Sci. Transl. Med.*, **4**, 127ps8.

Röthlisberger,D., Honegger,A. and Plückthun,A. (2005) *J. Mol. Biol.*, **347**, 773–789.

Santiago,C., Björling,E., Stehle,T. and Casasnovas,J.M. (2002) *J. Biol. Chem.*, **277**, 32294–32301.

Sanz,L., Kristensen,P., Blanco,B., Facteau,S., Russell,S.J., Winter,G. and Alvarez-Vallina,L. (2002) *Gene Ther.*, **9**, 1049–1053.

Schaefer,J.V. and Plückthun,A. (2012) *Protein Eng. Des. Sel.*, **25**, 485–506.

Théry,C., Ostrowski,M. and Segura,E. (2009) *Nat. Rev. Immunol.*, **9**, 581–593.

Wang,J.h. (2002) *Trends Biochem. Sci.*, **27**, 122–126.

Wilk,T., Gross,I., Gowen,B.E., Rutten,T., Haas,F., de Welker,R., Kräusslich, H.G., Boulanger,P. and Fuller,S.D. (2001) *J. Virol.*, **75**, 759–771.
Wörn,A. and Plückthun,A. (1998) *Biochemistry*, **37**, 13120–13127.
Wörn,A. and Plückthun,A. (2001) *J. Mol. Biol.*, **305**, 989–1010.
Zhou,Q., Schneider,I.C., Edes,I., *et al.* (2012) *Blood*, **120**, 4334–4342.
Zhu,Z.Y. and Blundell,T.L. (1996) *J. Mol. Biol.*, **260**, 261–276.
Zufferey,R., Nagy,D., Mandel,R.J., Naldini,L. and Trono,D. (1997) *Nat. Biotechnol.*, **15**, 871–875.